Photodissociation Dynamics in Ordered Monolayers: Physisorbed N_2O_4

Hugh Rieley,* Daniel J. Colby, Darren P. McMurray, and Stuart M. Reeman

Department of Chemistry, University of Liverpool, P.O. Box 147, Liverpool L69 3BX, U.K.

Received: January 27, 1997; In Final Form: March 24, 1997[⊗]

The dynamics of photodissociation in physisorbed N_2O_4 were investigated by time-of-flight mass spectrometry. Ordered monolayers were prepared by adsorption of NO_2 at 100 K on a water−ice surface of thickness *ca*. 30 monolayers held on a Cu(100) substrate. Irradiation of the sample surface at 355 nm resulted in exclusive desorption of NO_2 with a most probable fragment translational energy of *ca*. 17 meV. Irradiation at 532 nm produced no desorbing species. The NO_2 yield was linear in photon fluence, and the cross section for photodesorption was found to be $(9 \pm 2) \times 10^{-18}$ cm^2, similar to the gas phase absorption cross section at 355 nm. The angular distribution of the photodesorbed NO_2 was peaked sharply in a direction around 10° from the normal, and no fragments were detected at angles greater than 30° from the normal. The photodissociation dynamics are dependent on the unique properties of the physisorbed system. The optical absorption in the adsorbate corresponds to the $\tilde{B}^1B_{2u} \leftarrow \tilde{X}^1A_g$ transition in N_2O_4, as in the gas phase; however the subsequent dynamics in the excited state are markedly different from the gas phase counterpart. Despite the weak interaction with the substrate, significant energy transfer occurs in the ordered physisorbed monolayer to yield nascent NO_2 with very low translational energy and a constrained angle of escape which is consistent with a high degree of adsorbate order and alignment.

1. Introduction

It is well established that the gas−solid interface is a unique chemical environment in which the extent of the interaction between an adsorbate and the surface is crucial in determining the properties of the system. Photochemical experiments provide a means of studying the influence of this interaction. In cases where the surface is an electrical insulator, the adsorbate−substrate interaction is typically weak and direct absorption of a photon by the adsorbed species is invariably the initial reaction step.[1] Conversely, on metal surfaces optical excitation of the substrate is an inescapable fact and there are very few (if any) clear cut cases of direct excitation of a chromophore in a chemisorbed system leading to an observed photon driven process. In the vast majority of cases studied, excitation of charge carriers (usually electrons) in the substrate are found to dominate the observed photochemistry.[2] In physisorbed systems, since the initial step is essentially determined by the absorption spectrum of the free gas phase molecule, the photochemistry is expected to be little different from that which occurs in the gas phase. However, it is clear from previous studies of photochemistry in adsorbates on "inert" insulator substrates that although the gas phase data provides a useful reference, the dynamics in the adsorbed state can be radically different.[1] The restriction of the degrees of freedom of reagents on adsorption and an increase in their effective concentration (with coverage) may not only drastically change the energy disposal in the reaction but may also result in reaction pathways which are unseen in the analogous gas phase reaction.[3] In addition, although electronic interactions may be weak in physisorbed systems, there is often a preferred orientation exhibited by the adsorbate molecules both in the monolayer and multilayer regimes. A clear example of this can be found in the work of Polanyi *et al*. on the HBr/LiF(001) system.[4,5] In the current study we are concerned with the photochemistry of physisorbed systems and, in particular, the influence of two-dimensional ordering on the dynamics of dissociation.

Dinitrogen tetroxide is a weakly bound dimer of NO_2, characterized by two NO_2 groups whose geometrical parameters are virtually identical with those observed in free NO_2.[6] The equilibrium geometry of gas phase N_2O_4 is planar symmetric, D_{2h}, with an exceptionally long N−N bond length, which lies in the range 1.756−1.782 Å.[7] The bond dissociation energy is correspondingly weak, *ca*. 0.56 eV.[8,9] Photolysis of gas phase N_2O_4 with ultraviolet (UV) light results in the formation of two NO_2 fragments, one or both of which is produced in an excited state that fluoresces in the visible with a lifetime of *ca*. 60−90 μs.[8] The UV absorption of N_2O_4 exhibits a relatively unstructured spectrum which shows one peak at *ca*. 345 nm, a strong peak at *ca*. 186 nm, and a weak shoulder, suggesting the existence of an absorption band between 305 and 240 nm.[10]

A study by Sisk *et al*. emphasized assignment of the electronic states of NO_2 fragments generated by photolysis of jet-cooled N_2O_4 at 193, 248, and 351 nm.[11] The electronic states of nascent NO_2 were determined by analysis of dispersed fluorescence spectra. For 351 nm, close to the wavelength used in the work presented here, the photolysis was assigned to

$$N_2O_4 + h\nu\ (351\ \text{nm}) \rightarrow NO_2(\tilde{B}^2B_1) + NO_2(\tilde{X}^2A_1) \quad (1)$$

with the electronically excited $NO_2(\tilde{B}^2B_1)$ displaying several quanta of vibration in its ν_2(O−N−O) bending mode. The electronic transition compatible with production of the $^2B_1$ state was determined, from the N_2O_4/NO_2 correlation diagram of von Niessen *et al*.,[12] to be the σ to π^* ($6a_g$ to $2b_{2u}$) HOMO to LUMO transition. This assignment predicted a transition dipole moment which was perpendicular to the molecular N−N axis and implied an angular distribution of photofragments which was sharply peaked along the molecular axis.

In the case of nonmetallic surfaces, all reports to date indicate that the adsorption of NO_2 results exclusively in the formation of N_2O_4.[13,14] The formation of layers of condensed N_2O_4 on water−ice surfaces has recently been studied using grazing incidence FTIR and TPD by Rieley *et al*.[14] TPD spectra of ice layers exposed to NO_2 evidenced desorption of molecular N_2O_4 at a temperature of 140 K, 25 K below the desorption

* Corresponding author. E-mail: rieley@liv.ac.uk.

[⊗] Abstract published in *Advance ACS Abstracts,* June 1, 1997.

S1089-5647(97)00325-8 CCC: $14.00

temperature of the water−ice at 165 K. Analysis of the spectra revealed activation energies for desorption of N_2O_4 and H_2O of 39 kJ mol^{-1} (0.4 eV) and 44 kJ mol^{-1} (0.51 eV), respectively. RAIRS spectra of adsorbed N_2O_4 were in agreement with those reported by Koch *et al.*[15] and indicated formation of highly ordered N_2O_4 layers with the N−N bond oriented normal to the surface. There was no evidence for a reaction between N_2O_4 and the water−ice.

The photochemistry of adsorbed N_2O_4 has been studied on both insulator and metal surfaces.[13,14,16−19] The earliest study, by Bach *et al.*, was concerned with investigating changes in the N_2O_4 absorption spectra on adsorption at a LiF crystal surface.[16] The investigation of photodissociation dynamics of N_2O_4 adsorbed on a NO-passivated Pd(111) surface was reported by Hasselbrink and co-workers.[17−19] This study, which utilized laser-induced fluorescence (LIF) to investigate the internal energy of photoproducts, found that irradiation with pulsed laser light in the wavelength range 351−193 nm resulted solely in the photodesorption of NO, with a maximum cross section for NO production of 3×10^{-18} cm^2 at 193 nm (6.4 eV).

The dynamics of photodissociation of N_2O_4 adsorbed on a nonmetallic surface was first reported by Dixon-Warren *et al.*[13] Under 248 nm laser irradiation, the desorption of NO and NO_2 was observed for N_2O_4 adsorbed on LiF(001) at 100 K. The yield of both the NO and NO_2 fragments was seen to increase linearly with increasing photon flux. Analysis of the internal state distributions of ejected NO fragments by resonance-enhanced multiphoton ionization (REMPI) found NO fragments in vibrational levels $v = 0-7$. For $v > 0$, the mean fragment translational energy was 0.11−0.15 eV, while for $v = 0$, $\langle E_{trans} \rangle$ was *ca.* 0.05 eV.

In a recent study of the CW photochemistry of N_2O_4 adsorbed on an inert surface, we reported that irradiation of N_2O_4 adsorbed on a water−ice surface in the range 300−400 nm resulted in the dissociation of N_2O_4 and desorption of NO_2 from the surface.[14] The relative cross section for NO_2 photodesorption was found to follow the wavelength response of the gas phase N_2O_4 molecule, peaking at *ca.* 340 nm. A preliminary infrared analysis confirmed that there was no chemical interaction of the N_2O_4 with the ice substrate and that the adsorbate layer was ordered with the N−N bands aligned predominantly along the surface normal. In this work, we build on our earlier study by investigating the photodissociation dynamics in ordered layers of physisorbed N_2O_4. As previously, monolayer coverages of N_2O_4 were prepared on a water−ice substrate. Subsequently, the surface was exposed to pulsed laser radiation at 355 nm. The translational energy and angular distributions of the nascent NO_2 were probed using time-of-flight mass spectroscopy in conjunction with rotation of the sample. Dynamics were observed which are peculiar to the ordered and aligned adsorbate.

2. Experimental Section

2.1. Description of Apparatus. The experiments were performed in a high-vacuum apparatus which consisted of separate photolysis and detection chambers. The photolysis chamber was a low volume, *ca.* 5 L, vessel, pumped by a single 150 L s^{-1} diffusion pump, to give a base pressure after bakeout of *ca.* 1×10^{-9} Torr. The photolysis chamber was equipped with a high-vacuum leak valve and attached steel capillary doser, which allowed the sample to be exposed to measured amounts of vapor (NO_2 or H_2O) from a rotary pumped gas-handling manifold. The Cu(100) sample was mounted centrally in the chamber, suspended on 0.25 mm tungsten wire spot welded to two tungsten support rods. The tungsten rods were in turn connected via copper barrel connectors to two OFHC copper rods which passed from the vacuum through insulating ceramic feedthroughs into a stainless steel dewar. The dewar was attached to a differentially pumped 360° rotary mounting table. A K-type (Chromel-Alumel) thermocouple fixed into a small hole in the side of the copper crystal allowed measurement of the sample temperature using a digital thermometer. The sample could be cooled routinely to temperatures in the region of 100 K by filling the steel dewar with liquid nitrogen. The detection chamber was separated from the photolysis chamber by a machined blank flange fitted with a 3 mm aperture and was pumped by a 50 L s^{-1} turbo pump. Monitoring of the gas phase species evolved during photolysis was performed using a triple-filter quadrupole mass spectrometer (QMS).

The light source used for all experiments was a Quanta-Ray GCR 11 Nd:YAG laser equipped with harmonic separator to generate the second and third harmonics at 532 and 355 nm, respectively. The laser was operated in either single shot or repetitive mode (with a shot frequency of 10 Hz) to yield pulses of *ca.* 10 ns width. The laser beam exiting the harmonic separator was steered using two turning prisms through a UV-grade quartz window in the photolysis chamber onto the sample. The laser emitted pulses with a physical cross section of *ca.* 1 × 2 cm. An adjustable iris was used to select only the central uniform portion of the beam, giving a circular beam incident at the sample with diameter *ca.* 1 cm. The pulse energy of the laser was measured using an Ophir 10A-P power meter, with fluences ranging from 3.5 to 35 mJ cm^{-2} per pulse.

2.2. Methodology. The Cu(100) sample was first annealed to >800 K to remove any contamination remaining from previous experiments and then cooled to *ca.* 100 K by filling the steel dewar with liquid nitrogen (LN_2). Layers of water were then condensed on the copper surface. Triply distilled water was deaerated on a rotary-pumped gas-handling manifold and metered into the vacuum system through a leak valve and stainless steel capillary, the end of which was *ca.* 4 cm from the sample. The water vapor issued into the chamber at a total ion gauge pressure of *ca.* 10^{-8} Torr for the required time. The water dosage was expressed in langmuirs, where 1 langmuir = 10^{-6} Torr s. Overlayers of N_2O_4 were prepared in similar fashion. NO_2 (Argo International, 99%), held in a glass vial, was purified by freeze distillation and deaerated on the gas-handling manifold. The vial was then immersed in an ice−water bath before dosing to reduce the vapor pressure of NO_2. NO_2 was then allowed to issue into the chamber through the steel capillary for a time determined by the required dose (in langmuirs). Due to the corrosive nature and consequent long pump-down time for NO_2, experiments were not commenced until the partial pressure of NO_2, as monitored using the mass spectrometer, returned to the original residual level.

The sample was then irradiated with either 532 or 355 nm laser light for a number of laser shots. During irradiation, the mass spectrometer was used to monitor one of three species produced as a result of electron bombardment of neutral species in the ionizer: NO_2^+ ($m/z = 46$), NO^+ ($m/z = 30$), or H_2O^+ ($m/z = 18$). The signals from the mass spectrometer were amplified by a Keithley 427 variable gain current amplifier and collected by a LeCroy 9310 Dual 300 MHz digital oscilloscope, triggered directly by the "SYNC OUT" output of the laser, using a channel width of typically 5 ms. The oscilloscope collected 10 000 points per channel and was additionally used to sum average the signal for a determined number of laser shots. Time-of-flight (TOF) spectra were recorded for both single shot and for a five-shot summed average for each experiment. The

spectra were then transferred to a Macintosh IIci computer via a National Instruments GPIB-DMA computer interface.

2.3. Data Analysis. Prior to analysis, the TOF spectra were corrected for the flight time down the mass spectrometer, t_{ion}, using the published formula[20]

$$t_{ion} = d\sqrt{m/1.916E} \quad (2)$$

where d is the distance from ionizer to detector (in cm), m is the mass of the ion (in atomic mass units), and E is the ion extract voltage from the QMS ionisation region (7 V). It is desirable to measure QMS flight times *in situ*; however, since our QMS was not equipped with the appropriate electronics to allow this measurement, we resorted to the use of the above formula which had been applied in similar circumstances to our own. Accordingly, we have imposed a generous error bound on the flight time of 10 μs (approximately, the difference between the calculated QMS flight times for NO_2 and NO). For NO^+ ($m/z = 30$) and NO_2^+ ($m/z = 46$), t_{ion} was calculated to be 47 and 58 μs, respectively. These flight times were subtracted from the data to give the TOF, $P(t)$, of the neutral species. The data was then fitted, using a least mean squares fitting procedure, to a shifted Maxwell−Boltzmann distribution of the form

$$P(t) = a(t) + b\left(\frac{s}{t}\right)^4 \exp\left\{\frac{-m}{2kT}\left(\frac{s}{t} - v_0\right)^2\right\} \quad (3)$$

The parameter s is the sample to QMS ionizer distance (23 cm), v_0 is the stream velocity, T is the effective Boltzmann temperature of the distribution, and b is a scaling factor. The function $a(t)$ is an analytical expression which satisfactorily represented the constant and temporal components in the background signal. It had the following form:

$$a(t) = a_0 + a_1 \exp(a_2 t^2) - a_3 \exp(a_4 t^2) \quad (4)$$

The TOF spectra and fit were then converted to a translational energy distribution using the Jacobian $J_{t,E}$ given by[21]

$$J_{t,E} = \frac{t^2}{ms} \quad (5)$$

which accounted for the required density-to-flux conversion, due to the reciprocal dependence of the mass spectrometer ionization efficiency on the velocity of the neutral species entering the ionizer.

3. Results

3.1. Time-of-Flight Spectra. A typical TOF spectrum obtained for the photolysis of N_2O_4 adsorbed on ice is shown in Figure 1. The spectrum was obtained over a five-shot average for a 2 langmuir dose of NO_2 onto *ca.* 30 layers of water−ice, with the sample normal oriented 2° from the axis of the mass spectrometer. The sample was irradiated with 355 nm light at an incident energy density of 8.5 mJ cm^{-2}, with the mass spectrometer set to monitor $m/z = 30$ (NO^+). Under these conditions five or six laser shots were sufficient to remove all detectable trace of N_2O_4 from the irradiated region of the surface since subsequent laser pulses produced no detectable NO_2 yield. The spectrum clearly shows two features: a sharp peak with a maximum situated at *ca.* 600 μs superimposed on a broad rise. The latter feature, discussed in more detail below, had little effect on the most probable arrival time of the early feature, which was readily fitted to the Maxwell−Boltzmann function described above. The fitting routine was performed for a mass

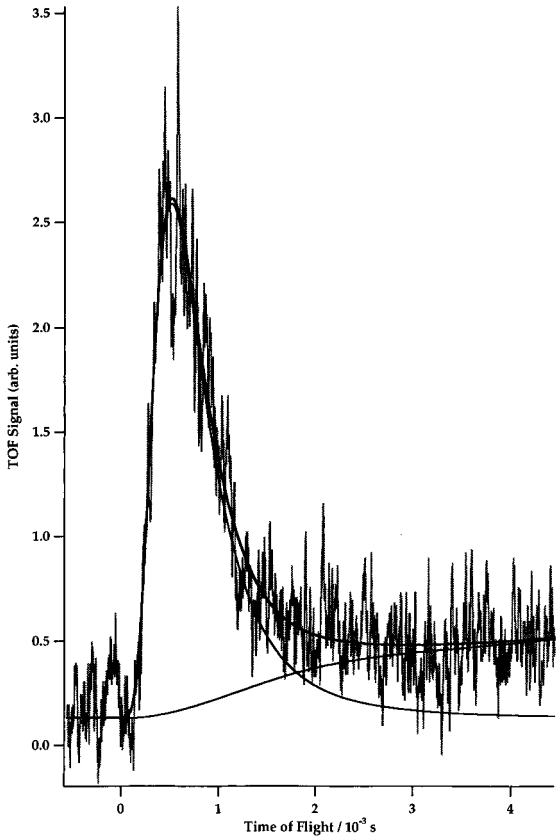

Figure 1. TOF spectrum of nascent NO_2 following the 355 nm (8.5 mJ cm^{-2}) irradiation of *ca.* 2 langmuir of N_2O_4 adsorbed on ice, as probed by the $m/z = 30$ (NO^+) cracking fragment. The solid lines represent the total fit to the data and the underlying Maxwell−Boltzmann and background components.

of 46 amu, i.e. NO_2, since a previous study of the CW photolysis of N_2O_4/ice concluded that this was the only species desorbed at this wavelength.[14] The identity of the desorbed species observed in these pulsed laser experiments was confirmed by comparison of the TOF spectra for $m/z = 30$ (NO^+) and $m/z = 46$ (NO_2^+) shown in Figure 2. The spectra were recorded for a 2 langmuir dose of NO_2 onto *ca.* 30 layers of ice with the sample normal oriented at an angle of 10° to the mass spectrometer axis. The decrease in the $m/z = 46$ (NO_2^+) signal is due to cracking into NO^+ in the mass spectrometer ionizer. Both spectra have been corrected for the relevant transit time through the mass spectrometer quadrupole, i.e. 47 μs for $m/z = 30$ and 58 μs for $m/z = 46$. The close similarity in temporal profiles of the two spectra and the good agreement between the ratio of the total yields and the cracking ratio of NO_2 (NO_2^+:$NO^+ \approx 1{:}3$) confirms that NO_2 only is ejected from the surface. It should be noted that species with $m/z = 76$ ($N_2O_3^+$), the stable daughter ion of $N_2O_4^+$, could not be detected, which indicated that desorption of the parent dimer did not occur.

Conversion from time-of-flight to energy distribution was performed on both the fit and the data using the Jacobian of eq 5. Analysis of the converted distributions revealed a peak, or most probable, translational energy of 17 ± 1 meV. The corresponding effective temperature for the distribution is *ca.* 200 K. This peak energy was found to be independent of laser fluence, adsorbate coverage, and the angle at which photodesorbed species were monitored. This latter point is illustrated in Figure 3, which shows TOF spectra and their corresponding energy distributions for three different detection angles. TOF spectra were also recorded using 532 nm irradiation in order to show that NO_2 was desorbed as a result of a photochemical

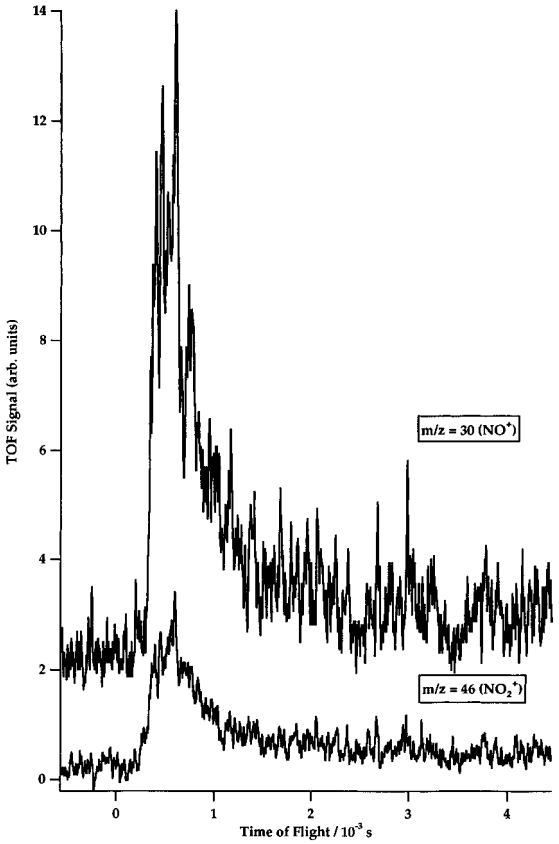

Figure 2. Comparison of TOF spectra taken under identical conditions for $m/z = 30$ (NO^+) and $m/z = 46$ (NO_2^+).

process at the surface. Figure 4 compares the TOF spectra obtained due to irradiation at 355 and 532 nm of 2 langmuirs NO_2 adsorbed on *ca*. 10 layers of ice. The laser energy density used in both experiments was 10 mJ cm^{-2}. In the case of the 532 nm trace, there is no detectable signal in the TOF spectrum, which indicates that the observed process is wavelength dependent and hence photochemical in nature.

3.2. Dependence of Yield on Laser Fluence. The effect of changing incident laser fluence on photodesorption yield was investigated for energy densities in the range 3.5−30 mJ cm^{-2}. The photodesorption yield was obtained from the TOF spectra by measurement of the area of the fitted short time feature. The graph, shown in Figure 5, demonstrates that the yield varies linearly with the number of photons incident at the surface, evidence of a single photon process. The possible ejection of H_2O from the ice layer was also monitored. However, over the range of laser fluences used in these experiments, no $m/z = 18$ (H_2O^+) signal was seen in the TOF signal, at either 355 or 532 nm.

3.3. Angular Dependence of Photodesorption Yield. The angular distribution of photodesorbed NO_2 was investigated for detection angles in the range 2−45°, where the detection angle (γ) is defined as the angle between the sample normal and the central axis of the mass spectrometer. It should be noted, however, that for these experiments, changing the detection angle also results in a change in the angle of incidence of the laser light (θ). Since the laser beam intersects the sample at right angles to the central axis of the mass spectrometer, the detection angle (γ) and the angle of incidence (θ) are related by $\theta = (90 - \gamma)$. The relevant geometry is shown in Figure 6b. Figure 6a shows the variation in photodesorption yield (described by the area of the fitted short time feature) as a function of detection angle, γ. Error bars have been added to the angular distribution to reflect the angular resolution of the experiment (*ca*. 4°) and the yield measurement (*ca*. 20% error). It is immediately apparent that the photodesorption yield of NO_2 occurs predominantly perpendicular to the surface. The angular distribution is very narrow with a peak at *ca*. 10° to the surface normal and a half-width of about 10°. No products attributable to a short time feature were detected for angles $\gamma > 30°$.

3.4. Coverage Dependence of Photodesorption Yield. The variation in photodesorption yield as a function of N_2O_4 coverage is shown in Figure 7. The measured yield for the first laser shot increased linearly for NO_2 doses in the range 0.5 to *ca*. 2 langmuirs. For higher NO_2 doses, the increase in photolysis yield was small. The linear region indicates that the photolysis cross section is constant with increasing coverage. The constancy of the yield for NO_2 doses higher than 2 langmuirs implies saturation of the photolysis occurs within the first molecular layer of N_2O_4.

3.5. Slow Feature in TOF Spectra. The slow feature observed in TOF for N_2O_4/ice was studied by analysis of the TOF spectra recorded for detection angles greater than *ca*. 45°. At such large angles, the short time feature discussed previously was absent, with only the long time rise in signal remaining, as shown in Figure 8a. The peak signal occurs at *ca*. 5 ms. The background feature was fitted to a function of the form given in eq 4, shown by the solid black line in Figure 8a. The integrated area of the long time feature, as a function of angle of detection, γ, is shown in Figure 8b. Consideration of the signal to noise ratio for the slow feature yielded an estimate of 12% for the error in calculated yield. Unlike the short time peak in the TOF spectra, which showed a distinct variation in yield with detection angle, the long time feature is unaffected by varying γ. Such a dependence on detection angle strongly suggests that the species responsible for the long time feature do not represent a nascent distribution of slow species exiting the surface. A more likely explanation for the origin of the slow feature is the detection of ejected photofragments following one or more collisions with the walls of the vacuum chamber. This rise in pressure in the photolysis chamber would be evidenced by a small increase in NO_2 background pressure in the detector region and is the source of the slow TOF feature.

3.6. Cross Section for NO_2 Photodesorption. The cross section for the photodesorption of NO_2 from N_2O_4 physisorbed on ice was calculated from the decrease in yield of the fast TOF feature from a one-shot to a five-shot averaged spectrum. A method was adopted which required estimation of neither surface coverage nor detector efficiency. A full explanation of the calculation procedure is given in the Appendix. The cross section for NO_2 photodesorption from physisorbed N_2O_4 at 355 nm was found to be $(9 \pm 2) \times 10^{-18}$ cm^2.

4. Discussion

The TOF spectra shown in Figures 1−3 provide clear evidence that irradiation of monolayers of N_2O_4 physisorbed on ice films results in the direct photodissociation of N_2O_4(ad) to yield nascent NO_2(g). As discussed previously, assignment of NO_2 as the sole ejected species was made by comparison of the TOF spectra for $m/z = 30$ (NO^+) and $m/z = 46$ (NO_2^+). For photodesorption of both NO and NO_2, the $m/z = 30$ spectra would be expected to be bimodal, i.e. there would be a contribution to the TOF signal from both ejected NO and NO_2. This is not observed: the TOF spectra shown in Figure 2 are identical in form. This absence of NO photodesorption is to be expected on energetic grounds, given that the wavelength threshold for production of NO fragments from the gas phase photolysis of N_2O_4 is *ca*. 320 nm.[22] TOF spectra recorded for

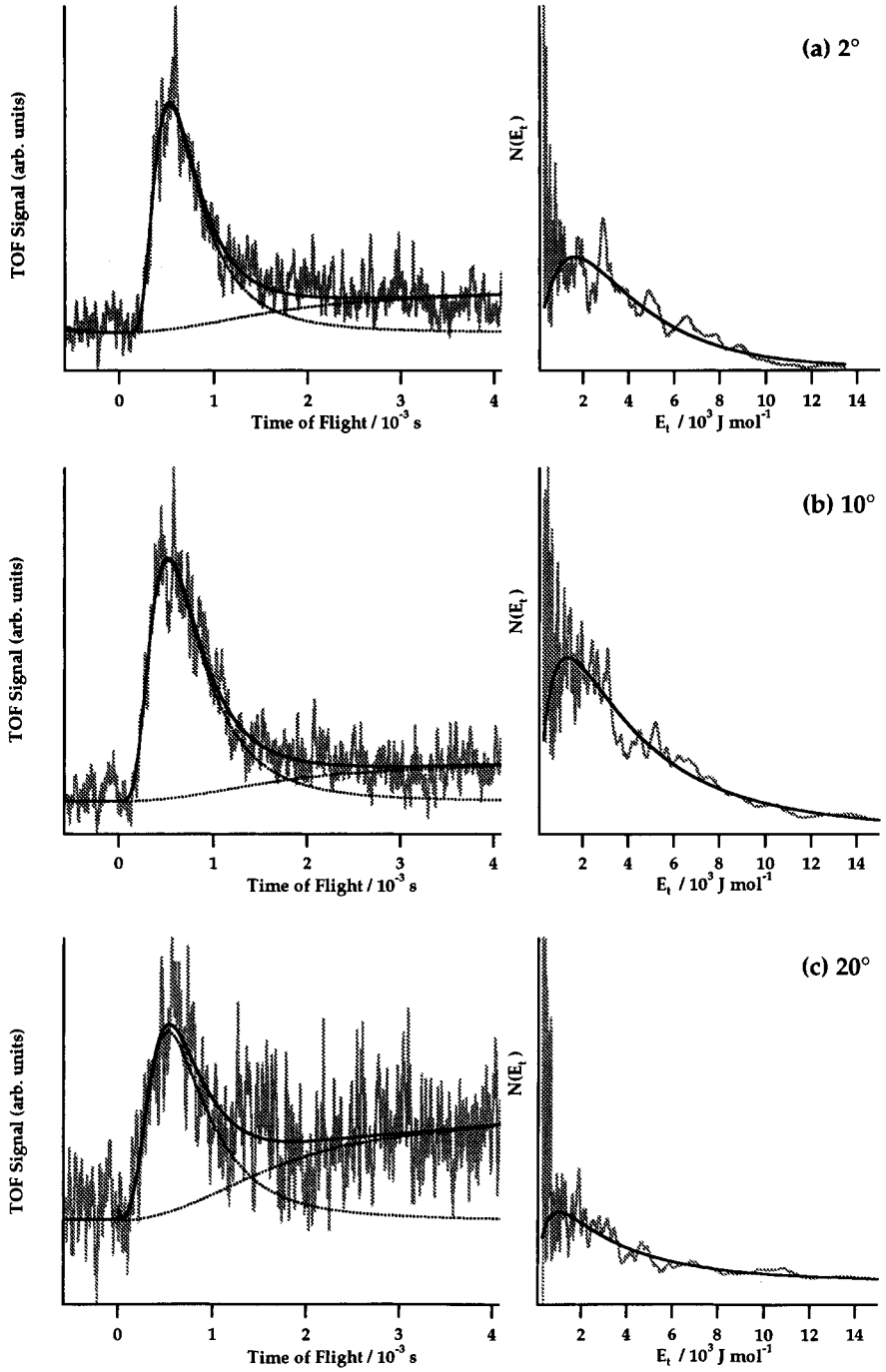

Figure 3. Time-of-flight and translational energy distributions following 355 nm irradiation of a *ca*. 2 langmuir dose of N_2O_4 adsorbed on ice at three different product detection angles. The solid line superimposed on the TOF data is the result of a nonlinear least squares fit. The solid line representing the energy distribution is an analytical transformation of this fit.

$m/z = 76$ ($N_2O_3^+$), the stable daughter product of $N_2O_4^+$, showed that no detectable desorption of the intact dimer occurred.

The excitation mechanism is assigned as direct photon absorption by the adsorbate. From Figure 4, comparison of the TOF spectra obtained for the same fluence of 355 and 532 nm light demonstrates clearly that the desorption of NO_2 from the ice surface is strongly wavelength dependent and hence photochemical in nature. For a mechanism involving laser heating of the surface, the desorption yield would be only weakly dependent on wavelength since the metal absorbance varies little for incident wavelengths ranging from the infrared to the ultraviolet.[23] Furthermore, detectable single-shot desorption of NO_2 is observed for laser fluences as low as 3.5 mJ cm^{-2}. Employing a formula for laser surface heating, published by Burgess *et al*.,[24] we calculate that the transient rise in surface temperature during the laser pulse is *ca*. 10 K. Hence the maximum surface temperature is *ca*. 120 K, which is below the *ca*. 140 K desorption temperature for N_2O_4.[14] It is worthwhile noting that since the N−N bond strength of the N_2O_4 dimer (*ca*. 0.5 eV[8]) is higher than the barrier to desorption (*ca*. 0.4 eV[14]), laser heating of the surface is unlikely to result in the exclusive production of NO_2(g), but would more likely lead to the desorption of molecular N_2O_4 which would be evident through the detection of the stable $N_2O_3^+$ daughter ion.

The presence of the underlying Cu(100) substrate in our experiments requires some consideration since it could potentially play an important role in the photodissociation dynamics. We contend that substrate-mediated photodesorption due to the temporary attachment of photoexcited metal electrons is not a

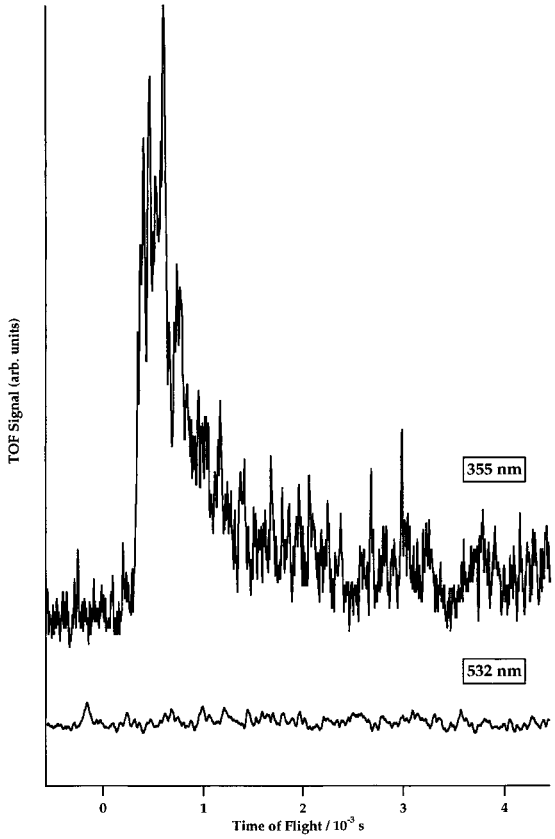

Figure 4. TOF spectra obtained from irradiation of *ca*. 2 langmuir of N_2O_4 adsorbed on ice with 355 nm (top trace) and 532 nm (lower trace) laser light.

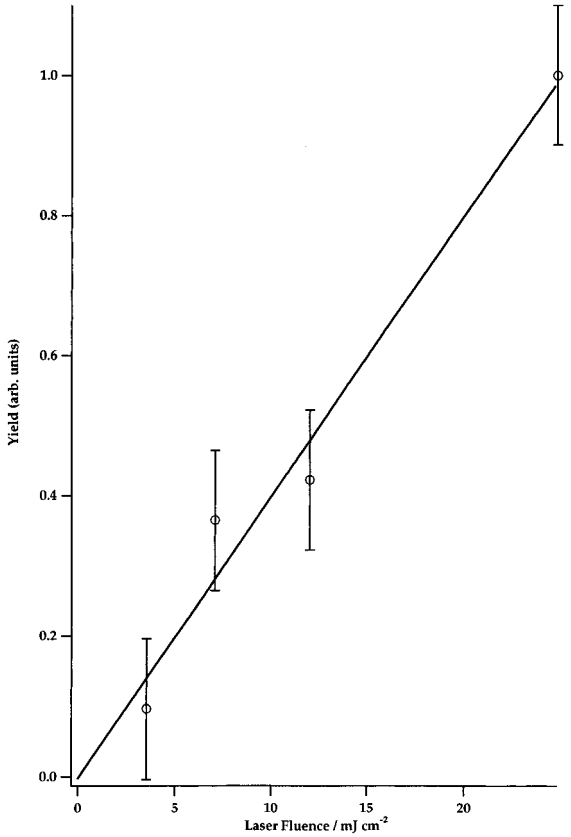

Figure 5. Variation of photodesorption yield with 355 nm laser fluence incident at surface. In each case, the surface was prepared with *ca*. 2 langmuir of N_2O_4 adsorbed on ice.

viable mechanism for photolysis of N_2O_4 adsorbed at the ice surface. It is known that the flux of excited electrons incident at an adsorbate is strongly attenuated by the presence of molecular spacer layers such that, for spacers of 10 layers or more, substrate-mediated photochemistry is no longer observed.[25−27] Given that ejection of NO_2 is detected in this work for ice spacers of *ca*. 30 layers, a substrate-mediated mechanism cannot account for the photodesorption of NO_2 from N_2O_4/ice. We must also consider, but will discount, the variation in the electric field intensity at the metal surface as being solely responsible for the observed angular distribution of photodesorbed NO_2. The surface electric field intensity (E_0^2/cos θ, where θ is the angle of incidence of the light) goes through a maximum around 80° for Cu,[28] which is coincident with the peak observed in the angular distribution at $\gamma = 90 - \theta = 10°$. If the form of the electric field intensity were the dominant factor, then the total photodesorption yield would be expected to fall sharply on either side of this maximum. We note two experimental observations which mitigate against the calculated metal electric field intensity playing a dominant role in the dynamics. In the first instance, at all angles studied ($2° \leq \gamma \leq 90°$) the adsorbate layer was removed within five laser shots. Since the metal electric field intensity is much lower at higher values of γ, the photodesorption efficiency is expected to be lower and the adsorbate layer should survive for a greater number of laser shots than at $\gamma = 10°$ where the intensity is much higher. The second piece of evidence is presented in Figure 8b, which shows that the integrated yield of the background component of the TOF spectra is *independent* of angle γ. As stated in the Results section, we believe this feature to be due to the detection of desorbed NO_2 which reaches the detector following collision with the walls of the reaction chamber. The functional form of this part of the distribution defies its assignment to a dynamical process at the surface. However, since the angular acceptance of the detector is only *ca*. 4°, this signal is therefore representative of the *total* desorbed yield at each angle. If the metal electric field intensity were solely responsible for dictating the desorption yield, this background component would follow the same variation with angle: it clearly does not.

Given that the electric field intensity of the underlying metal surface does not appear to play the dominant role in driving the dynamics of photodissociation in adsorbed N_2O_4, we explore the effect of direct dissociation in two-dimensionally ordered layers. Sisk *et al*.,[11] following a photolysis study of N_2O_4 in the gas phase, found that 351 nm irradiation (close to the wavelength used in the present study) resulted in the dissociation of the N−N bond and the production of one electronically excited and one ground state NO_2 fragment. The electronic transition induced by 351 nm light absorption was determined to be the σ to π^* HOMO to LUMO transition, which has an electronic transition dipole moment oriented perpendicular to the N−N bond axis, i.e., $\tilde{B}^1B_{2u} \leftarrow \tilde{X}^1A_g$. This assignment of a perpendicular transition moment implied an angular distribution of photofragments (in a randomly oriented gas phase sample) at 90° to the direction of the electric vector of the incident radiation.[11]

The results of previous adsorption studies of N_2O_4 harbour two important conclusions which are of importance here. Firstly, TPD measurements showed that the interaction of N_2O_4 with water−ice surfaces is weak, with a desorption activation energy of *ca*. 40 kJ mol^{-1}—typical of a physisorption interaction.[14] Secondly, FTIR spectroscopy of thin films formed by adsorbing NO_2 on gold at 80 K[15] and on water/Cu(100) at 100 K[14] showed that NO_2 dimerizes on weakly interacting surfaces at low temperature to form an ordered layer of N_2O_4 in which

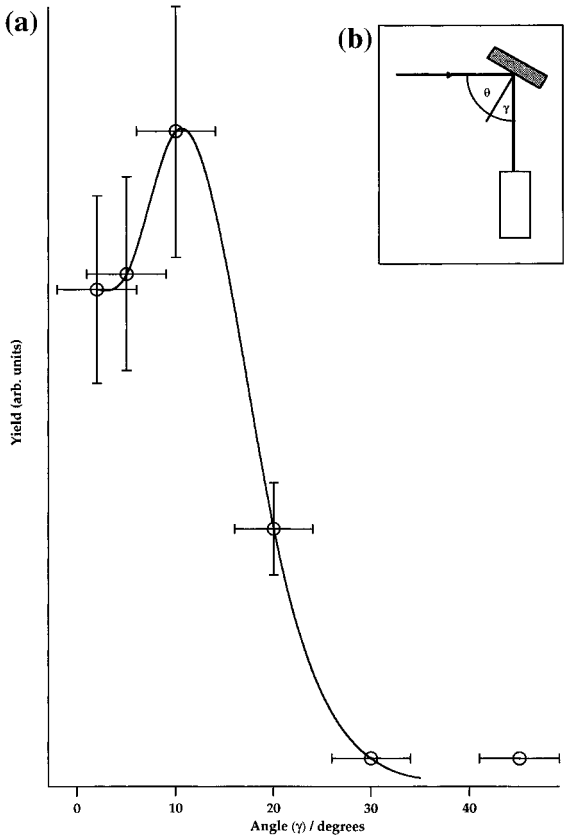

Figure 6. Angular distribution of photodesorbed NO_2. (a) Product angular distribution as a function of γ. (b, inset) Relation between angle of detection (γ) and laser angle of incidence (θ).

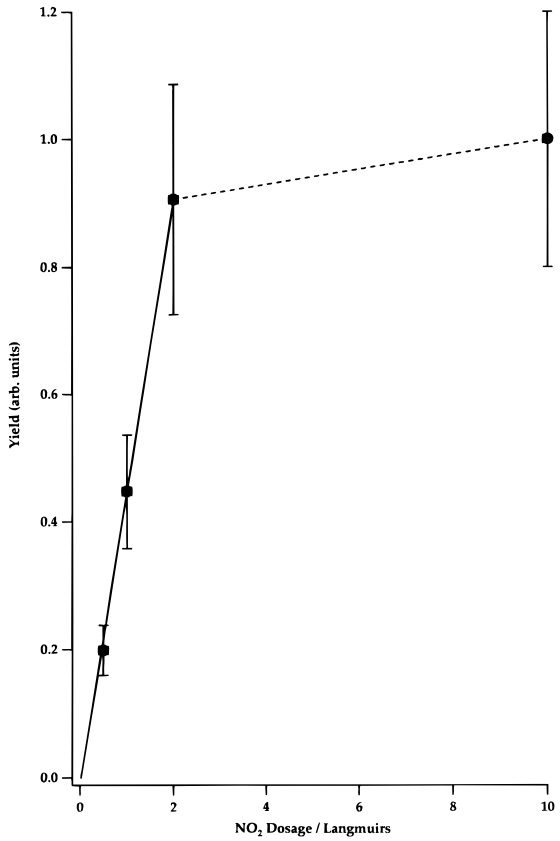

Figure 7. Variation of photodesorption yield with N_2O_4 coverage (expressed as NO_2 dosage in langmuirs).

the N−N bonds are aligned predominantly perpendicular to the surface. This was reasoned on the basis of a comparison of gas phase and adsorbed phase infrared spectra. On adsorption, either directly on a metal surface or on a thin multilayer of water separated from an underlying metal substrate, infrared absorption due to vibrations perpendicular to the N−N axis in N_2O_4 (of B_{2u} symmetry) was severely quenched, while those parallel to the N−N axis remained strong. Reference to the metal−surface selection rule of Pearce and Sheppard[29] provided the physical rationale for this behavior: dipole changes parallel to the metal surface are quenched while those perpendicular to the surface are enhanced, and therefore the C_2 axis (N−N bond axis) must lie predominantly along the surface normal. The strong, narrow features which remained in the FTIR spectrum testified to the high degree of crystalline order in the N_2O_4 layer(s).[14,15]

Since, in the case of the current work, the adsorbate is physisorbed to the ice surface, we assume that there is no significant modification of the electronic structure of the adsorbed N_2O_4 molecule compared to the free gas phase species. Rupture of the N−N bond in ordered and aligned N_2O_4 physisorbed on ice is expected to result in the desorption of NO_2 from the surface with an angular distribution which is peaked close to the normal. The measured angular distribution of ejected NO_2 photofragments, shown in Figure 6, is indeed peaked toward the surface normal, with a maximum occurring at *ca.* 10°, consistent with the expected distribution for direct photolysis as discussed above. The fact that the maximum in this distribution does not appear to lie precisely along the surface normal indicates that the N−N bonds in the adsorbate are canted away from the normal by an average of some 10°. This is supported by the grazing incidence FTIR spectra taken of N_2O_4 adsorbed on gold at 80 K[30] and on ice at 100 K,[14] in which the detection of the asymmetric B_{2u} mode (whose dipole moment change is parallel to the surface) suggests that the molecules are not aligned with their N−N bonds perfectly along the surface normal. The angular distribution of the desorbing NO_2 is remarkably narrow. This is attributed to a high degree of order and alignment in the adsorbate, which serves to constrain the range of angles made by the N−N bonds to the surface normal and, therefore, the angle of escape of the photofragments. This behavior is distinct from that exhibited by a randomly aligned gas phase sample of N_2O_4, which, for a perpendicular transition,[11] is expected to result in a $\sin^2\theta$ distribution of photofragments, where θ is the angle between the electric vector of the incident radiation and the direction of the breaking bond.[31]

The observed N_2O_4 coverage dependence of the photolysis yield is shown in Figure 7. The measured yield of ejected NO_2 increases linearly for initial NO_2 doses in the range *ca.* 0 to 2 langmuirs. For NO_2 doses above *ca.* 2 langmuirs, the photolysis yield curve levels off with increasing coverage. From the work of Rieley *et al.*,[14] this switching point corresponds to the completion of the first molecular layer of N_2O_4. The linear region indicates that the photolysis cross section is constant with respect to N_2O_4 coverage, while the essentially constant yield for coverages higher than 1 monolayer ($\approx$2 langmuir dose) indicates that only species present in the top monolayer contribute to the observed yield of NO_2(g). Such a coverage dependence is consistent with the photodesorption of NO_2 from physisorbed N_2O_4. Photolysis of molecules from underlying layers will not contribute to the measured yield since the kinetic energy available for escape of the nascent NO_2 fragments (*ca.* 17 meV) is less than the desorption activation energy of the overlying N_2O_4 condensate (*ca.* 0.4 eV).[14] The linear increase in photodesorption yield for sub-monolayer coverages indicates that the degree of intermolecular interaction in the condensate, while being sufficient to cause ordering, does not significantly perturb the individual N_2O_4 species at higher coverages. The

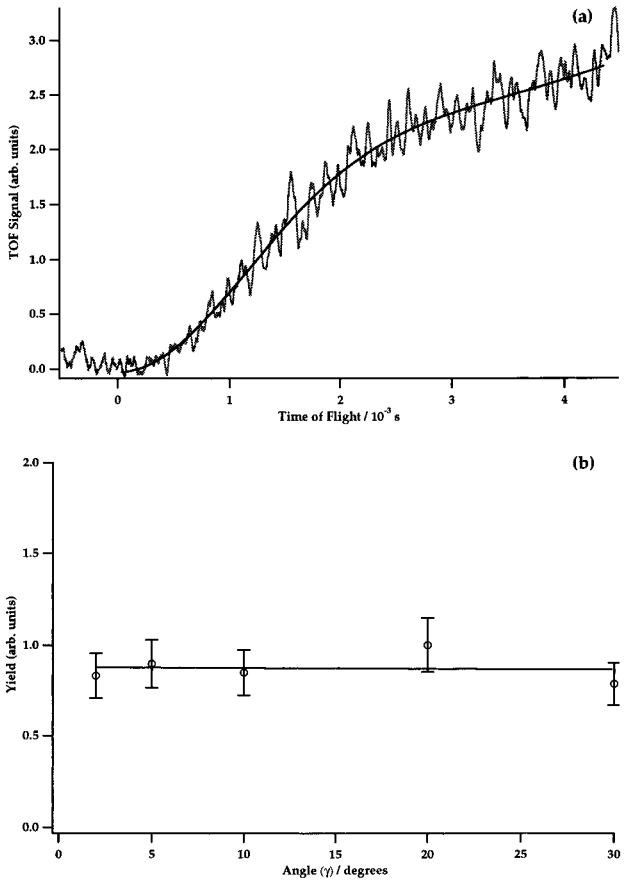

Figure 8. Slow feature seen in TOF spectra. (a) The temporal profile at $m/z = 30$ (NO^+) at a detection angle of 45°. (b) The variation of the integrated signal with detection angle γ.

good agreement between the measured cross section for photodesorption of NO_2 (*ca.* 19×10^{-18} cm^{-2}) and the gas phase absorption cross section[32] (*ca.* 17×10^{-18} cm^{-2}) is further evidence that there is little perturbation of N_2O_4 on adsorption.

The linear dependence of N_2O_4 yield on laser fluence, shown in Figure 5, is indicative of a one-photon process. Such a linear dependence, for the energy densities used in this study (3.5−35 mJ cm^{-2}), is consistent with a direct absorption excitation mechanism. Direct excitation involving two-photon absorption has been observed previously in surface photochemistry but with a corresponding quadratic dependence of photodesorption yield on laser fluence, for example in the two photon photodesorption of CO^+ at 193 nm from CO/Pt(111).[33] The absence in the TOF spectra of any feature which may be ascribed to photodesorbed NO leads to the conclusion that the two-photon mechanism described by Dixon-Warren *et al.* for the photolysis of N_2O_4/LiF(001)[13] is not operative for N_2O_4 adsorbed at the ice surface.

Information concerning the dynamics of NO_2 desorption via photolysis of physisorbed N_2O_4 can be obtained from the TOF spectra presented in Figure 3. The peak, or most probable, translational energy for NO_2 desorption was found to be *ca.* 17 meV, with a corresponding effective Boltzmann temperature of *ca.* 200 K. The total available energy resulting from the absorption of a single 355 nm photon is 3.49 eV, while the energy required to dissociate N_2O_4 to two ground state NO_2 molecules is 0.56 eV,[34] leaving 2.93 eV available for partitioning among all the degrees of freedom of the photofragments. Following the work of Sisk *et al.*,[11] the 355 nm photolysis of gaseous N_2O_4 must result in the formation of one ground state and one excited state NO_2 fragment. The evidence presented above leads us to believe that the same is true for physisorbed N_2O_4. The formation of NO_2 ($\tilde{B}^2B_1$) requires a further 1.83 eV of energy, to leave 1.1 eV available energy. In the gas phase photolysis at 351 nm, a significant proportion (*ca.* 33%) of the available energy is manifest as photofragment translational energy.[20] However, in the case of a molecule adsorbed on a surface, the opportunity exists for excess energy to be transferred to the substrate, which acts as an efficient energy sink, to produce photofragments of translational energy lower than that of their gas phase counterparts. It is worth pointing out here that the energetic threshold to the production of $NO(X^2\Pi) + O(^3P)$ from $NO_2(\tilde{X}^2A_1)$ is 3.11 eV.[35] Therefore, at 355 nm there is insufficient energy to produce photofragment NO, which is consistent with our experimental observations.

Comparing this work with that of Dixon-Warren *et al.*,[13] it is clear that the 355 nm photodissociation of N_2O_4 physisorbed on ice produces NO_2 fragments with a similarly low fraction (*ca.* 1.5%) of the available energy in translation as does the 248 nm photolysis of N_2O_4 adsorbed on LiF(001) (*ca.* 2%). The 248 nm study also highlights the complexities involved when exciting at shorter wavelengths,[36] since the production of NO becomes an important competing pathway. A possible explanation for the lower fraction of the available energy in translation of desorbed NO_2 fragments in the present study is an increase in quenching rate for electronically excited N_2O_4 by solid water compared to an LiF substrate. Such increased quenching could occur due to the presence of the Cu(100) substrate beneath the ice layers, which introduces the possibility of electromagnetic field coupling of excited state N_2O_4 to the metal surface. The lifetime of the excited state is inversely proportional to the cube of the distance of the adsorbate from the metal.[37,38] However, there was no change in the TOF spectra of photodesorbed NO_2 for N_2O_4 adsorbed on ice coverages in the range 10−30 layers. This increase in spacer thickness corresponds to a *ca.* 100 Å increase in the separation of N_2O_4 and the Cu surface, taking one ice layer to be *ca.* 5 Å thick.[38] Such a change in separation, from 50 to 150 Å, should result in a *ca.* 25-fold decrease in the decay rate of the N_2O_4 excited state due to field coupling. If field coupling were effective in quenching the N_2O_4 excited state, such a reduction in efficiency would be manifested as a change in the TOF spectra. That dipole coupling is not effective is perhaps a little surprising, given that field-coupling theory predicts excited state lifetimes for adsorbates in the range 10^{-13}−10^{-12} s,[39] compared to the time scale for bond dissociation, which is *ca.* 10^{-13} s.[40] However, since the measured cross section for NO_2 desorption from N_2O_4/ice/Cu(100) is the same, within expected error, as the gas phase absorption cross section, it is clear that quenching is not effective in this system. For this reason, quenching of excited state N_2O_4 by intermolecular electronic energy transfer to the ice surface or to surrounding N_2O_4 adsorbate species is also ruled out, especially as the predicted excited state lifetime for such a process, *ca.* 10^{-12} s,[39] is longer than that for dipole quenching.

The most likely explanation for the low NO_2 photofragment translational energy is provided by a consideration of momentum transfer to the respective substrate during the dissociation process. For N_2O_4/LiF(001), the adsorbate is bound to a crystalline solid. Hence, during dissociation, the NO_2 fragment which remains at the surface is held by the rigid substrate lattice, and thus the departing fragment receives a higher fraction of the available kinetic energy. Since the crystal lattice is resistant to deformation, momentum transfer to the surface is small. For N_2O_4 physisorbed on ice, the substrate is an amorphous condensate which is capable of considerably greater deformation than the LiF crystal. For comparison, the standard lattice enthalpy of crystalline LiF is *ca.* 1036 kJ mol^{-1},[23] while the

enthalpy of sublimation of H_2O ice is *ca*. 40 kJ mol^{-1}.[1,23,41] During the photolysis of N_2O_4 at the ice surface, the bound NO_2 fragment is not stationary since the ice surface will deform under the dissociative impulse. Consequently there is expected to be significant momentum transfer to the ice surface with a corresponding reduction in the kinetic energy available to the departing NO_2 fragment.

Taking together the information regarding the order and alignment in the physisorbed N_2O_4, as determined by previous FTIR measurements,[14,15] and the results from this dynamical study, we are able to construct a mechanism for the photolysis of N_2O_4(ad) at 355 nm. The adsorbate is comprised of physisorbed N_2O_4, which exhibits a high degree of crystalline order and predominant alignment of N−N bonds along the surface normal. Photodissociation of this bond following absorption at 355 nm is likely driven by direct optical excitation of the $\tilde{B}^1B_{2u} \leftarrow \tilde{X}^1A_g$ transition, similar to that in gaseous N_2O_4.

Photodesorption of NO_2 occurs along the direction of the N−N bond and, therefore, perpendicular to the surface. Unfortunately, due to the current experimental geometry it is not possible to determine the direction of the electronic transition dipole moment and thereby confirm the identity of the excited state. Future experiments, in which a polarized laser beam is directed at grazing incidence along the axis of rotation of the sample manipulator, will resolve this issue.

5. Summary

The photochemistry of N_2O_4 adsorbed on ice/Cu(100) has been investigated. Irradiation with 355 nm laser light results in the photodesorption of NO_2, with peak translational energy of 17 ± 1 meV and a measured cross section of (9 ± 2) × 10^{-18} cm^2. No photochemical processes are observed at 532 nm. The photodesorption yield is linear in laser fluence and linear in surface coverage—although saturation occurs in the latter case on completion of the first monolayer. A direct optical excitation mechanism is identified as being responsible for the desorption of NO_2. The angular distribution of photodesorbed NO_2 is peaked sharply, centered at *ca*. 10° to the surface normal with a half-width of *ca*. 10°. The dynamics are consistent with the constraints imposed by a tightly packed, ordered monolayer in which the N_2O_4 molecules are aligned with the N−N axes canted at an average of 10° to the surface normal and in which significant energy transfer occurs between the electronically excited state and the surface.

Acknowledgment. We are grateful for the financial support of the EPSRC under Grant GR/H10573 and to the NERC under Grant GST/02/860 and to the CLRC for the loan of the Nd:Yag laser. We also thank the Department of Education for Northern Ireland for the provision of a studentship for D.P.M. and EPSRC for studentships for D.J.C. and S.M.R.

Appendix: Calculation of Cross Section for Photodesorption

The cross-section for photolysis of N_2O_4 physisorbed ice is calculated by consideration of the shot to shot decrease in the photodesorption yield of NO_2. The method employed compares the measured yield from single-shot and five-shot summed average laser experiments for identical conditions. The single-shot value is taken from the first shot of the five-shot average. Such an approach is advantageous in that it avoids complicating factors such as evaluation of the efficiency of the detection system used to obtain the data (in this case a mass spectrometer), which are inherent in other methods.

It is assumed that any attenuation of the incident light flux is due solely to absorption in the adsorbed layer and that this gives rise exclusively to photodesorbed NO_2 (i.e. unit quantum efficiency for photodissociation). Then, for any incident laser pulse, the ratio of the number of incident to nonabsorbed photons will be given by the Beer−Lambert expression:

$$\frac{N_{ph} - N_{diss}}{N_{ph}} = \exp\{-\sigma(\lambda)N_{ads}\} \quad \text{(A1)}$$

N_{ph}, N_{diss}, and N_{ads} are the number of incident photons, the number of molecules which dissociate, and the number of adsorbate species, respectively, per unit area, and $\sigma(\lambda)$ is the cross section for photodesorption of NO_2. In the limit that $\sigma(\lambda)N_{ads} \ll 1$, which, taking the gas phase absorption cross section to be *ca*. 7 × 10^{-18} cm^2 (from Harwood and Jones[32]) and monolayer coverage to be *ca*. 10^{15} cm^{-2}, is a reasonable approximation in this case, this expression simplifies to

$$N_{diss} = \sigma(\lambda)N_{ph}N_{ads} \quad \text{(A2)}$$

Alternatively, since the integrated yield is proportional to the number of adsorbate molecules which dissociate, we may write the yield for the first laser shot as

$$\text{yield}(1) \propto N_0\sigma(\lambda)N_{ph} \quad \text{(A3)}$$

Similarly, the total yield over five laser shots (obtained from the five-shot summed average) can be written as

$$\text{yield}(5) \propto [N_0 + N_1 + N_2 + N_3 + N_4]\sigma(\lambda)N_{ph} \quad \text{(A4)}$$

where N_n is the number density of adsorbed N_2O_4 molecules after n laser shots.

The ratio of the one- and five-shot yields, $R_{1:5}$, is given by

$$\frac{\text{yield}(1)}{\text{yield}(5)} = \frac{N_0}{[N_0 + N_1 + N_2 + N_3 + N_4]} = R_{1:5} \quad \text{(A5)}$$

and hence

$$N_0 + N_1 + N_2 + N_3 + N_4 = \frac{N_0}{R_{1:5}} \quad \text{(A6)}$$

Since the photolysis cross section is constant with changing N_2O_4 coverage, as discussed above, the fraction, a, of adsorbed N_2O_4 depleted per laser shot is constant. The coverage after n laser shots expressed as a function of the initial coverage is then given by

$$N_1 = \frac{N_0}{a}, \quad N_2 = \frac{N_1}{a} = \frac{N_2}{a^2}, \quad ..., \quad N_n = \frac{N_0}{a^n} \quad \text{(A7)}$$

Equation A6 can now be expressed in the form

$$N_0 + \frac{N_0}{a} + \frac{N_0}{a^2} + \frac{N_0}{a^3} + \frac{N_0}{a^4} = \frac{N_0}{R_{1:5}}$$

Alternatively

$$1 + \frac{1}{a} + \frac{1}{a^2} + \frac{1}{a^3} + \frac{1}{a^4} = \frac{1}{R_{1:5}} \quad \text{(A8)}$$

The sum to the nth part of the series $\sum_n 1/a^n$ is given by[42]

$$\sum_n \frac{1}{a^n} = \frac{1 - \left(\frac{1}{a}\right)^n}{1 - \frac{1}{a}} \tag{A9}$$

and hence,

$$\sum_0^4 \frac{1}{a^n} = \frac{1 - \left(\frac{1}{a}\right)^4}{1 - \frac{1}{a}} \tag{A10}$$

Substitution into eq A8 yields

$$\frac{a - a^{-3}}{a - 1} = \frac{1}{R_{1:5}} \tag{A11}$$

Solving eq A11 numerically then gives the fractional depletion in coverage per laser shot, a. Given the fractional depletion in coverage, the number density of N_2O_4 at the surface after five shots is given by

$$N_5 = N_0/a^5 \tag{A12}$$

and hence the total number of species depleted by the five laser shots, N_{dep}, is

$$N_{dep} = N_0 - N_0/a^5 \tag{A13}$$

The cross section for photodesorption of NO_2 from the photolysis of N_2O_4(ad) can now be expressed as

$$\sigma = \frac{N_{dep}}{N_0 N_{ph}} = \frac{N_0 - N_0/a^5}{N_0 N_{ph}} = \frac{1 - 1/a^5}{N_{ph}} \tag{A15}$$

Consequently, given a relative change in photodesorption yield the photolysis cross section can be calculated solely from the shot to shot diminution in NO_2 photodesorption yield. No estimation of the initial number density of N_2O_4 at the surface or the detection efficiency of the mass spectrometer is necessary. For the example in question the relative difference between the first-shot and five-shot summed yield gives a value for $a = 2.7 \pm 0.3$ and $\sigma = (9 \pm 2) \times 10^{-18}$ cm^2.

References and Notes

(1) Polanyi, J. C.; Rieley, H. Photochemistry in the Adsorbed State. In *Dynamics of Gas-Surface Collisions*; Ashfold, M. N. R., Rettner, C. T., Eds.; The Royal Society of Chemistry: London, 1991; p 326.

(2) Zhou, X.-L.; Zhu, X.-Y.; White, J. M. *Surf. Sci. Rep.* **1991**, *13*, 73.

(3) Dixon-Warren, S. J.; Matyjaszczyk, M. S.; Polanyi, J. C.; Rieley, H.; Shapter, J. G. *J. Phys. Chem.* **1991**, *95*, 1333.

(4) Bourdon, E. B. D.; Cho, C. C.; Das, P.; Polanyi, J. C.; Stanners, C. D.; Xu, G. Q. *J. Chem. Phys.* **1991**, *95*, 1361.

(5) Cho, C. C.; Polanyi, J. C.; Stanners, C. D. *J. Phys. Chem.* **1988**, *92*, 6859.

(6) C. W. Bauschlicher, J.; Komornicki, A.; Roos, B. *J. Am. Chem. Soc.* **1983**, *105*, 745.

(7) Kvick, A.; McMullan, R. K.; Newton, M. D. *J. Chem. Phys.* **1982**, *76*, 3754.

(8) Patten, K. O., Jr.; Burley, T. D.; Johnston, H. S. *J. Phys. Chem.* **1990**, *94*, 7960.

(9) Giauque, W. F.; Kemp, J. D. *J. Chem. Phys.* **1938**, *67*, 81.

(10) Bass, A.; Ledford, J.; Laufer, A. H. *J. Res. Natl. Bur. Stand.* **1975**, *80*, 143.

(11) Sisk, W. N.; Miller, C. E.; Johnston, H. S. *J. Phys. Chem.* **1993**, *97*, 9916.

(12) von Niessen, W. D.; Cedarbaum, L. S.; Schirmer, J. *J. Chem. Soc., Faraday Trans. II* **1978**, *74*, 1556.

(13) Dixon-Warren, S. J.; Polanyi, J. C.; Rieley, H.; Jackson, R. C.; Shapter, J. G.; Weiss, H. *J. Phys. Chem.* **1992**, *96*, 10983.

(14) Rieley, H.; McMurray, D. P.; Haq, S. *J. Chem. Soc., Faraday Trans.* **1996**, *92*, 933.

(15) Koch, T. G.; Horn, A. B.; Chesters, M. A.; McCoustra, M. R. S.; Sodeau, J. R. *J. Phys. Chem.* **1995**, *99*, 8362.

(16) Bach, W.; Breuer, H. D. *Discuss. Faraday Soc.* **1974**, *58*, 237.

(17) Hasselbrink, E. *Appl. Phys. A* **1991**, *53*, 403.

(18) Hasslebrink, E.; Jakubith, S.; Nettesheim, S.; Wolf, M.; Cassuto, A.; Ertl, G. *J. Chem. Phys.* **1990**, *92*, 3154.

(19) Ertl, G.; Hasselbrink, E. *Mol. Phys.* **1992**, *76*, 777.

(20) Harrison, J. A.; Yang, X.; Rösslein, M.; Felder, P.; Huber, J. R. *J. Phys. Chem.* **1994**, *98*, 12260.

(21) Nishi, N.; Shinohara, H.; Okuyama, T. *J. Chem. Phys.* **1984**, *80*, 3898.

(22) Kawasaki, M.; Kasatani, K.; Sato, H. *Chem. Phys.* **1983**, *78*, 65.

(23) *Handbook of Chemistry and Physics*; Lide, D. R., Ed.; CRC Press: Boca Raton, 1992; Vol. 73.

(24) Burgess, J. D.; Stair, P. C.; Weitz, E. *J. Vac. Sci. Technol., A* **1984**, *4*, 1362.

(25) Marsh, E. P.; Tabares, F. L.; Schneider, M. R.; Gilton, T. L.; Meier, W.; Cowin, J. P. *J. Chem. Phys.* **1990**, *92*, 2004.

(26) Marsh, E. P.; Gilton, T. L.; Meier, W.; Schneider, M. R.; Cowin, J. P. *Phys. Rev. Lett.* **1988**, *61*, 2725.

(27) Jo, S. K.; White, J. M. *J. Chem. Phys.* **1991**, *94*, 5761.

(28) Hollins, P.; Pritchard, J. *Prog. Surf. Sci.* **1985**, *19*, 275.

(29) Pearce, H. A.; Sheppard, N. *Surf. Sci.* **1977**, *59*, 205.

(30) Koch, T. G.; Horn, A. B.; Chesters, M. A.; McCoustra, M. R. S.; Sodeau, J. R. *J. Phys. Chem.* **1995**, *99*, 8362.

(31) Zare, R. N.; Herschbach, D. R. *Proc. IEEE* **1963**, *51*, 173.

(32) Harwood, M. H.; Jones, R. L. *J. Geophys. Res. D* **1994**, *99*, 22955.

(33) Fukutani, K.; Song, M.-B.; Murata, Y. *J. Chem. Phys.* **1995**, *103*, 2221.

(34) Kerr, J. A. *Chem. Rev.* **1966**, *66*, 5761.

(35) Okabe, H. *Photochemistry of Small Molecules*; Wiley: New York, 1978.

(36) Dixon-Warren, S. J.; Polanyi, J. C.; Rieley, H.; Jackson, R. C.; Shapter, J. G.; Weiss, H. *J. Phys. Chem.* **1992**, *96*, 10983.

(37) Chance, R. R.; Prock, A.; Silbey, R. *J. Chem. Phys.* **1975**, *62*, 2245.

(38) Chance, R. R.; Prock, A.; Silbey, R. *Adv. Chem. Phys.* **1978**, *37*, 1.

(39) Avouris, P.; Walkup, R. E. *Annu. Rev. Phys. Chem.* **1989**, *40*, 173.

(40) Beswick, J. A. *Chem. Phys. Lett.* **1990**, *168*, 246.

(41) Thiel, P. A.; Madey, T. E. *Surf. Sci. Rep.* **1987**, *7*, 211.

(42) Jeffrey, A. *Mathematics for Engineers and Scientists*, 4th ed.; Van Nostran Reinhold: London, 1989.